WPS1-CPR(18) 20584

D Gradic et al.

Doppler coherence imaging of impurity flows in the divertor of tokamaks and stellarators

Preprint of Paper to be submitted for publication in Proceeding of 30th Symposium on Fusion Technology (SOFT)

This work has been carried out within the framework of the EUROfusion Consortium and has received funding from the Euratom research and training programme 2014-2018 under grant agreement No 633053. The views and opinions expressed herein do not necessarily reflect those of the European Commission.

A new calibration implementation for Doppler Coherence Imaging Spectroscopy

Dorothea Gradic[a], Valeria Perseo[a], Ralf König[a], David Ennis[b], the W7-X team[a]

[a]*Max-Planck-Institut für Plasmaphysik, Wendelsteinstr. 1, D-17491 Greifswald, Germany*
[b]*Auburn University, Auburn, USA*

Abstract

A new widely tunable, continuous-wave laser named C-Wave enables direct calibration at the un-shifted, center-of-mass wavelength for all visible plasma lines in the range between 450 and 650 nm for Doppler Coherence Imaging Spectroscopy. It also provides the ability to scan around each desired wavelength on a small range of ±50 pm, thus enabling an easy way to translate the measured phase difference $\Delta\Phi$ of the diagnostic into the desired Doppler line shift $\Delta\lambda$, that corresponds to the physical parameter of interest, the particle velocity of an observed plasma species.
A first wavelength scan of the C-Wave laser ±50 pm around a single plasma line of interest, C III at 464.881 nm, is presented and compared to a simulated wavelength scan. It demonstrates not only the C-Wave capability as a Doppler CIS calibration source, but also its potential to immensely simplify Doppler CIS analysis for nearly all visible plasma lines of interest.

Keywords: Doppler Coherence Imaging Spectroscopy

1. Introduction

Doppler Coherence Imaging Spectroscopy (CIS), a relatively new ([1]) and powerful method to measure 2-dimensional images of line-of-sight integrated particle velocity flows and temperatures from a light-radiating body such as a plasma, is increasingly used in high-temperature plasma experiments such as DIII-D ([2]), MAST ([3]), ASDEX Upgrade ([4]) and Wendelstein 7-X ([5]). It measures a single emission line from the plasma, with which a spatial interference pattern is produced by a set of birefringent plates on a camera chip. To analyse the measured plasma line interference pattern, a reference interference pattern is produced with a monochromatic calibration line. Ideally, these calibration lines are at the unshifted, center-of-mass position of the observed plasma line, λ_0. Strong (impurity) plasma lines of interest in the visible part of the light spectrum include e.g. C III, C II, He II and many other lines from higher excitation stages. However, these atomic emission lines usually cannot be generated with conventional spectral calibration lamps. This is why for many observed plasma lines, calibration wavelengths in the vicinity of a few nanometers to λ_0 are used. An example is the C III multiplet at 464.881 nm, for which a Zn I calibration line at 468.014 nm is usually used. In these cases, the analysis of the $\Delta\Phi \rightarrow \Delta\lambda$-relation becomes much more difficult for the Doppler CIS, since additional phase effects, generated by the birefringent plates of the Doppler CIS, have to be considered.

Previous calibration methods rely on spectral lamps, laser diodes and conventional lasers that drastically limit the availability of close, intense calibration lines. By the use of an unshifted calibration line ($\lambda_{\texttt{cali}} = \lambda_0$), additional analysis terms can be omitted. With the small-range scanning capability of the laser in a range of ±50 pm, which is corresponding to the range of expected Doppler line shifts of the particle species in the edge of a high-temperature plasma experiment, the sign of the $\Delta\Phi \rightarrow \Delta\lambda$-relation can be determined without doubt for the applied plate configuration. Furthermore, the need for simulating any birefringent plate parameters dissolves completely. This is also true for multiplet emission lines such as C III, that generate an additional multiplet phase offset ([7]), if those multiplets are measured with the C-Wave laser as well.

A newly developed, widely tunable continuous-wave (CW) laser (called 'C-Wave') based on optical parametric oscillation (OPO) provides monochromatic line emission over nearly the entire visible spectrum (450-525 nm and 540-650 nm) and the near infra-red (900-1300 nm) ([6]). For Doppler CIS, the C-Wave laser was specifically customized to apply precise wavelength selection with an accuracy of < 0.1 pm and wavelength scanning in a range of ±50 pm around a chosen wavelength λ_0 with a newly developed software tool called "AbsoluteLambda", that involves the application of a high-resolution wavemeter. With this new calibration source, several issues with conventional calibration methods for CIS can be dealt with:

1. All plasma lines in the range of 450-525 nm and 540-650 nm can be absolutely calibrated at their non-shifted, center-of-mass line position.
2. With the small-range scanning capability of the laser (in a range of ±50 pm), the $\Delta\Phi \rightarrow \Delta\lambda$-relation for CIS can be directly measured for each Doppler CIS plate configuration and does not have to be simulated anymore.

The tunable C-Wave laser is used as a calibration source for the two Doppler CIS systems on Wendelstein 7-X, during the current operation phase 1.2 b. In this work, a first wavelength scan of the C-Wave laser ±50 pm around a single plasma

line of interest, C III at 464.881 nm, is presented and compared to a simulated wavelength scan. This is done to demonstrate it's capability as a Doppler CIS calibration source, immensely simplifying the complex CIS analysis procedure, that has been described in many previous works ([11], [7], [8]) and will not be discussed here.

2. Wavelength scan with the tunable laser

As reported in [5], there are two Doppler CIS systems used in W7-X, that observe the same divertor area from different view ports, enabling better understanding of the line-integrated emission and flow patterns. Those two systems are named after the ports from which they observe the plasma, AEQ21 and AEF30, and they also apply different birefringent plate configurations. The thickness, material and type of plates determine the fringe phase shift for an observed emission line wavelength. The more or thicker plates are used, the smaller wavelength shifts can be resolved. A small-range wavelength scan with the C-Wave was performed with the two W7-X Doppler CIS systems simultaneously to assess the phase dependence on wavelength for both systems. This was done with a Y-fibre at the output of the C-Wave laser, with which the calibration spheres of the two systems were connected to the laser each. With another Y-fibre, a He-Ne laser source was connected to both CIS calibration spheres in the same way.

The entire wavelength scan lasted for several minutes. However, even in the time span of a few minutes, ambient temperature changes of and around the birefringent plates can be present. The birefringent plate refractive indices, n_e and n_o, that determine the phase shift of the incident light on the plate, are not only dependent on the wavelength, but also the material temperature. Therefore, ambient temperature changes around the plates can change and distort the measured phase. Since the two Doppler CIS set-ups on W7-X do not involve an active or passive temperature control for the birefringent plates (e.g. via temperature cells or ovens), no temperature control was used during the laser wavelength scan either. To assess temperature effects on the measured phase difference during the C-Wave wavelength scan, an additional (fixed) wavelength was measured simultaneously to monitor the overall temperature effect on the phase difference. As additional fixed wavelength, a He-Ne laser line at 632.8163 nm was used. As was reported in ([8], p.68), two distinct wavelengths can be successfully measured with the same Doppler CIS camera at the same time if they form two separable peaks in Fourier space. The distance of two peaks in Fourier space depends on the wavelengths and the fringe size. The tunable laser wavelength was set to the un-shifted center-of-mass wavelength of the C III multiplet at 464.8811 nm and varied in a range of ±50 pm around it. In Figure 1, the interferometer signal generated by the two monochromatic laser wavelengths is shown. It consists of two overlaying modulation patterns. For the two W7-X systems, the wavelength peaks of the two lasers (632.8 nm - 464.9 nm = 167.9 nm) proved to be separated enough in Fourier space, as can be seen in Figure 2. The simultaneous measurement of two wavelengths goes at the cost of spatial resolution, since the inverse Fourier transform area becomes smaller.

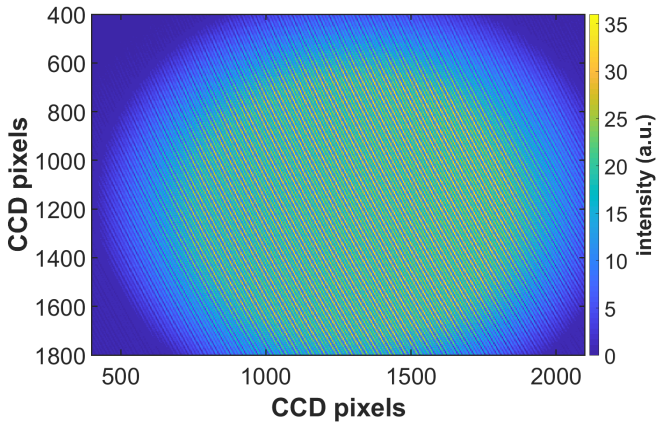

Figure 1: Doppler CIS interferometer signal recorded with the C-Wave laser (started at 464.881 nm) and the HeNe ion laser (632.816 nm), taken from the AEF30 port CIS system.

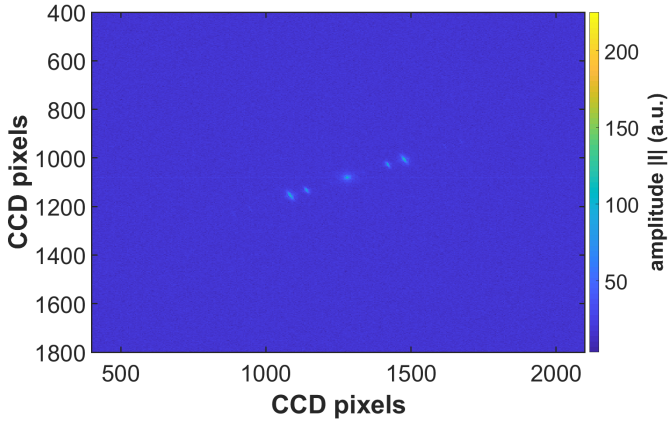

Figure 2: 2D Fourier transform image of the interference pattern in Figure 1.

The two Doppler CIS systems observe the W7-X plasma from two different observation points ([5]) and employ different plate configurations in OP1.2b. The AEQ21 system consists of a 10 mm α-Barium Borate (α-BBO) displacer plate, the second system in AEF30 applies a 10 mm α-BBO displacer plate and a 5.4 mm α-BBO delay plate. In Figures 3 and 4, the temporal evolution of the tunable laser phase difference and the He-Ne laser phase difference are shown for both Doppler CIS systems during the wavelength scan. First, the tunable laser wavelength was decreased and increased in 5 pm steps, then 10 pm steps several times around the center-of-mass wavelength of the C III multiplet at 464.881 nm, which was set as reference point ($\Delta\lambda = 0$ pm). As expected, the phase increase is stronger for the AEF30 system, which has an additional delay plate. However, in that system, the temperature drift of the phase is slightly higher, corresponding to $\Delta\Phi \approx 2$ over 10 minutes for the He-Ne line. The recorded temperature change in the AEF30 sys-

tem was ΔT =??C. At AEQ21, $\Delta\Phi \approx -0.2$ over 10 minutes for the He-Ne line, since the temperature change and the phase dependence were less in this system. In AEQ21, the sign of the $\Delta\Phi$-$\Delta\lambda$-relation was opposite to the one in AEF30, since the orientation of the birefringent displacer plate axis was different.

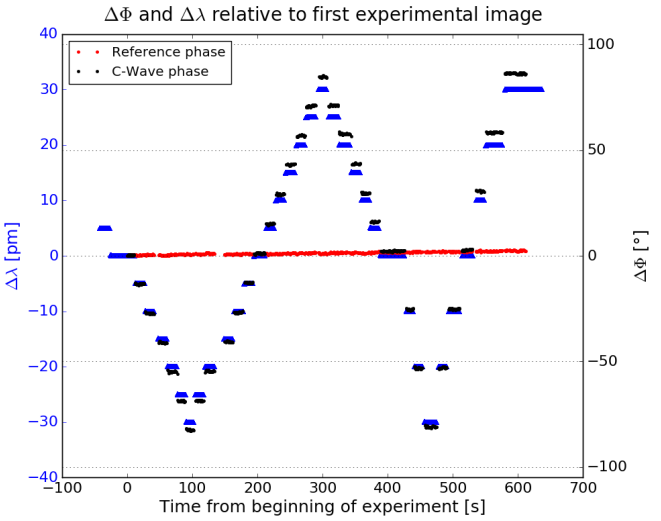

Figure 3: C-Wave wavelength scan of the Doppler CIS set-up used in W7-X port AEF30. Displayed are the wavelength of the C-Wave (blue), the averaged measured phase difference of the (fixed) He-Ne laser (red) and the phase difference of the C- Wave (black). The $\Delta\Phi$ averages were taken in the central area of the Doppler CIS images (marked in Figure **??**). As reference phase image, the first measurement image was taken for both wavelengths, respectively.

The effect of the temperature-induced phase drift, which differs for different wavelengths, appears to be stronger for light in the blue part of the spectrum than in the red. This was reported in [8] and was also observed in this wavelength scan experiment, although the overall phase drift was much smaller since only α-BBO plates were used. The temperature-induced phase drifts for the C-Wave laser phase was slightly higher at $\lambda_0 = 464.881$ nm, being ??. With the ratio of those two drifts, the phase drift for the C-Wave phase can be estimated for the whole scan experiment and subtracted from the measured phase to extract the measured $\Delta\Phi \rightarrow \Delta\lambda$-relation, which can be seen in Figure 5.

Figure 5 shows the measured $\Delta\Phi \rightarrow \Delta\lambda$-relation for both W7-X Doppler CIS systems, which operate with different plate configurations. In the AEF30 system, a positive phase corresponds to a blue shifted line (or flow towards the observer), whereas in the AEQ21 system, it corresponds to a flow away from the observer. For comparison, a simulated $\Delta\Phi \rightarrow \Delta\lambda$-relation has been added to the Figure to quantify theoretical predictions. The simulated phase shift due to a birefringent delay or displacer plate can been calculated according to ([9]):

$$\Phi(\theta = 0) = \frac{2\pi L}{\lambda_0}\left[(n_o - n_e) - \frac{\sin^2\alpha}{2n_o}\left(1 + \frac{n_e}{n_o}\left[1 - \sin^2\delta\left(1 - \frac{n_e^2}{n_o^2}\right)\right]\right)\right] \quad (1)$$

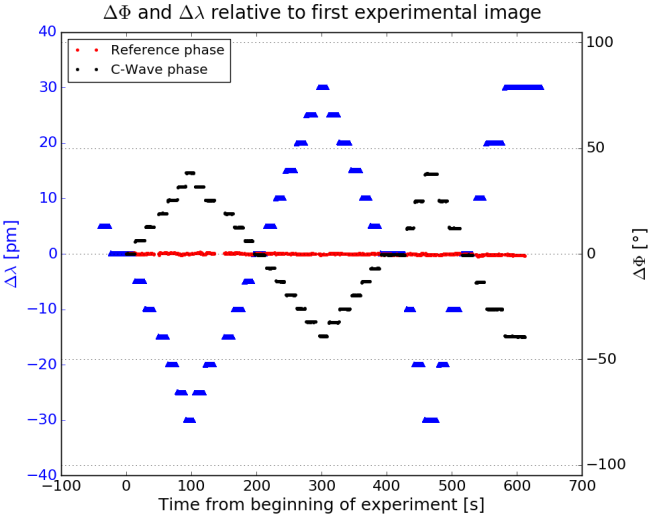

Figure 4: C-Wave wavelength scan of the Doppler CIS set-up used in W7-X port AEQ21. Displayed are the wavelength of the C-Wave (blue), the averaged measured phase difference of the (fixed) He-Ne laser (red) and the phase difference of the C- Wave (black). The $\Delta\Phi$ averages were taken in the central area of the Doppler CIS images (marked in Figure **??**). As reference phase image, the first measurement image was taken for both wavelengths, respectively.

$$\Phi(\theta = 45) = \frac{2\pi L}{\lambda_0}\left[\frac{(n_o - n_e)}{2} + \frac{\left(n_o^2 - n_e^2\right)}{\left(n_o^2 + n_e^2\right)}\cos\delta\sin\alpha\right] \quad (2)$$

where n_e, n_o are the birefringent indices for the material in use (here: α-BBO, provided in [10]). L is the thickness of the birefringent plate, θ the orientation of the birefringence axis, α is the angle between the incident light and the plate surface and δ is the angle between the projections of the incident light and the optical axis on the plate surface. The plate parameters, which were applied to the best of the authors knowledge (relying on manufacturer data) need to be known with a high degree of accuracy. Small uncertainties cause phase offsets that might affect how $\Delta\Phi$ changes for a given Doppler shift $\Delta\lambda$. As can be seen in the Figure, the agreement between the measured and simulated $\Delta\Phi \rightarrow \Delta\lambda$-relation is high, demonstrating the validity of the model. This comparison might also be used to fit the plate parameters for simulations, as has been suggested by [11].

3. Summary and Conclusion

An important assumption for the Doppler CIS analysis with previously applied calibration sources, where $\lambda_{\texttt{cali}} \neq \lambda_0$, is that $\Delta\Phi$ for a certain Doppler shift $\Delta\lambda$ can be accurately predicted. This requires the birefringent indices n_e, n_o to be accurately known. Furthermore, diagnostic parameters such as the thickness of the birefringent plates, the orientation of the birefringent plate axes, the camera chip pixel where $\alpha = 0$ and focal length f of the CCD lens need to be known with very high precision. These small uncertainties cause phase offsets that can distort the $\Delta\Phi \rightarrow \Delta\lambda$-relation. Under these circumstances, it is

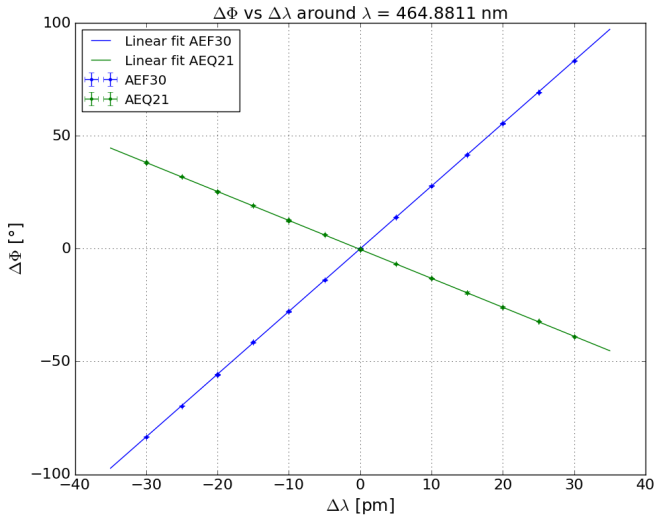

Figure 5: The measured and simulated $\Delta\Phi \rightarrow \Delta\lambda$-relations for both W7-X CIS sytems in AEF30 and AEQ21.

not impossible to analyse measured phase data ([11], [4]), however it involves a time-consuming process to identify the precise plate parameters for each new plate configuration or even small changes to the same set-up. With the C-Wave laser as a new calibration source for Doppler CIS, all plasma lines in the range of 450-525 nm and 540-650 nm can be directly calibrated at their center-of-mass position. As has been demonstrated in this work, the $\Delta\Phi \rightarrow \Delta\lambda$-relation can be directly measured with C-Wave, confirming the accuracy of previous simulation codes as well as omitting the need for simulating any phases for Doppler CIS in the future, thus making analysis much faster and trivial.

4. Acknowledgments

The authors would like to thank Auburn University for their funding and support for the W7-X Doppler CIS.
This work has been carried out within the framework of the EUROfusion Consortium and has received funding from the Euratom research and training programme 2014-2018 under grant agreement No 633053. The views and opinions expressed herein do not necessarily re ect those of the European Commission.

References

[1] J. Howard, Coherence imaging spectro-polarimetry for magnetic fusion diagnostics, J. Phys. B: At. Mol. Opt. Phys. 43 (2010) 144010 (10pp)
[2] J. Howard, A. Diallo, et al., Coherence Imaging of Flows in the DIII-D Divertor, Contrib. Plasma Phys. 51, No. 2-3 (2011) 194 200
[3] S.A. Silburn, J.R.Harrison, J. Howard, et al., Coherence imaging of scrape-off-layer and divertor impurity flows in the Mega Amp Spherical Tokamak, Rev. Sci. Instrum. 85 (2014) 11D703
[4] D. Gradic, O.P. Ford, et al., Doppler coherence imaging of divertor and SOL ows in ASDEX upgrade and Wendelstein 7-X, Plasma Phys. Control. Fusion 60 (2018) 084007 (12pp)
[5] V. Perseo, et al., Coherence Imaging Spectroscopy systems on Wendelstein 7-X for studies of island divertor plasma behavior, 44th EPS Conf. on Plasma Phys. 41F (2017) 5.103
[6] J. Sperling and K. Hens, Made Easy: CW Laser Light Widely Tunable across the Visible
[7] PhD Thesis S.A. Silburn: A Doppler Coherence Imaging Diagnostic for the Mega-Amp Spherical Tokamak
[8] PhD Thesis D. Gradic: Doppler Coherence Imaging of Ion Dynamics in VINETA.II and ASDEX Upgrade
[9] F.E. Veiras, L.T. Perez, M.T. Garea, Phase shift formulas in uniaxial media: an application to waveplates, Applied Optics 49(15) (2010) 2769-77
[10] K. Kato, Second-Harmonic Generation to 2048 Å in β-BaB_2O_4, IEEE Journal of Quantum Electronics 22(7) (1986) 1013-4 (1987)
[11] C. Samuell, S.L. Allen, W.H. Meyer and J. Howard, Absolute calibration of Doppler coherence imaging velocity images, Journal of Instrumentation 12 (2017) C08016